ACS APPLIED MATERIALS & INTERFACES

Letter

www.acsami.org

High-Energy-Density Sol–Gel Thin Film Based on Neat 2-Cyanoethyltrimethoxysilane

Yunsang Kim,[†,‡,§] Mohanalingam Kathaperumal,[†,‡] O'Neil L. Smith,[†,‡] Ming-Jen Pan,[⊥] Ye Cai,[‡,§] Kenneth H. Sandhage,[‡,§] and Joseph W. Perry*[,†,‡]

[†]School of Chemistry and Biochemistry, [‡]Center for Organic Photonics and Electronics, and [§]School of Materials Science and Engineering, Georgia Institute of Technology, Atlanta, Georgia 30332, United States

[⊥]Naval Research Laboratory, 4555 Overlook Avenue, Washington, D.C. 20375, United States

Supporting Information

ABSTRACT: Hybrid organic–inorganic sol–gel dielectric thin films from a neat 2-cyanoethyltrimethoxysilane (CNETMS) precursor have been fabricated and their permittivity, dielectric strength, and energy density characterized. CNETMS sol–gel films possess compact, polar cyanoethyl groups and exhibit a relative permittivity of 20 at 1 kHz and breakdown strengths ranging from 650 V/μm to 250 V/μm for film thicknesses of 1.3 to 3.5 μm. Capacitors based on CNETMS films exhibit extractable energy densities of 7 J/cm^3 at 300 V/μm, as determined by charge–discharge and polarization-electric field measurements, as well as an energy extraction efficiency of ~91%. The large extractable energy resulting from the linear dielectric polarization behavior suggests that CNETMS films are promising sol–gel materials for pulsed power applications.

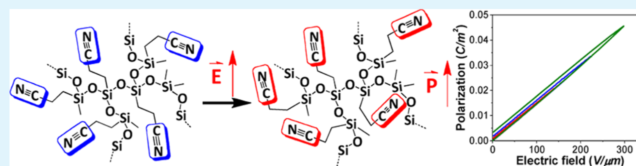

KEYWORDS: *sol–gel dielectric, high k dielectric, high energy density materials, capacitors, electric breakdown strength, pulsed power applications*

INTRODUCTION

With the ever-increasing demand for electrical energy, there is great interest in high-performance energy storage materials and devices, such as capacitors, supercapacitors, batteries, and fuel cells.[1−5] Among these devices, capacitors have an intrinsic advantage for high power density because of their fast electrical charge and discharge responses. The performance of capacitors is limited by the characteristics of the dielectric storage material including: its permittivity, electrical loss, breakdown strength and statistics, and processability.[6,7] Traditionally, polymeric thin film capacitors have been used to meet requirements because of their large breakdown strength, which typically exceeds 300 V/μm, and their fast charge/discharge speeds on the order of microseconds.[8] However, conventional polymeric dielectric materials suffer from low relative permittivity that substantially limits the energy storage density of capacitors.[9] To improve the relative permittivity of polymeric materials, researchers have focused substantial efforts on the development of materials such as ferroelectric polymer-based films,[10−12] nanocomposites based on both ferroelectric polymers and high permittivity inorganic nanoparticles,[5−7,13,14] and sol–gel hybrid materials.[15,16] Although these approaches have yielded significant improvement in the relative permittivity and energy density of materials for capacitors, the need for the development of materials that possess high permittivity, large breakdown strength, low loss at high electric field, high reliability, and facile processability remains.

The organic–inorganic hybrid sol–gel approach is a promising method for the formation of dielectric films, as it offers relatively mild reaction conditions for the synthesis of composite materials with molecular level control of composition and solution-based processing of films.[17,18] One avenue to develop sol–gel hybrid materials with high permittivity is to incorporate highly polarizable moieties as a pathway to high energy density materials. Recently, Kwon et al. reported on organic–inorganic sol–gel hybrids in which surface-modified $BaTiO_3$ nanoparticles were incorporated into organic–inorganic sol–gel hybrid matrices.[15] Their sol–gel hybrids were formed by the hydrolysis and the condensation of trimethoxysilane with pendant acrylate groups, which were polymerized following condensation. 4,4′-(hexafluoroisopropylidene)diphenol was also included to impart a moderate dipole moment and electronic polarizability. The hybrid sol–gel composites with 65 and 400 nm $BaTiO_3$ particles showed relative permittivities of ~25 and ~62, respectively, at 1 kHz. The dielectric strength of the composite with 65 nm $BaTiO_3$ particles was reported to be 263 V/μm, quite similar to poly(vinylidene fluoride-*co*-hexafluoropropylene)-$BaTiO_3$ nanocomposites.[14]

Another pathway to high permittivity hybrid sol–gel films would be to incorporate compact dipolar groups tethered to a

Received: December 18, 2012
Accepted: February 21, 2013
Published: February 21, 2013

 © 2013 American Chemical Society

trimethoxysilane precursor via a flexible linkage, which could provide for a dipolar orientation polarization mechanism. An example of such organic sol−gel hybrid materials was reported by Maruyama, et al. based on xerogel films prepared from blends of trialkoxysilanes, tetraalkoxysilanes and a trialkoxysilane with a pendant cyanoalkyl-moiety, which showed large relative permittivity in the range of 22 to 27 and small loss tangent, along with good thermal and mechanical stability.[16]

In this paper, we report on the formation of neat sol−gel films of 2-cyanoethyltrimethoxysilane (CNETMS, Figure S1a in the Supporting Information) and a detailed study of their morphology, electronic and dielectric properties that are crucial to evaluate the potential for energy storage applications. We have fabricated xerogel films (1.3 to 3.5 μm in thickness) of CNETMS and characterized the permittivity, electric breakdown strength, Weibull statistics, extractable energy density and loss. The polarization mechanism of CNETMS sol−gel films has been examined via polarization-electric field (P-E) measurements, which show narrow P-E loops, suggesting the potential of CNETMS sol−gel films as linear dielectrics for pulsed-power and energy storage applications.

■ RESULTS AND DISCUSSION

CNETMS Film Morphology and Dielectric Properties. Films of CNETMS were prepared with thicknesses ranging from 1.3 to 3.5 μm as determined by profilometry. Infrared spectroscopy confirms the presence of cyano, −OH, $-CH_2-$ and Si−O−Si vibrational absorption bands (see Figure S2a in the Supporting Information). The morphology of CNETMS films was characterized using AFM, top surface and cross-sectional SEM and cross-sectional transmission electron microscopy (TEM) imaging. AFM images (see Figure S3 in the Supporting Information) of CNETMS films exhibit a very smooth surface with an RMS roughness of 0.27 nm. SEM images (see Figure S4a,b in the Supporting Information) and XRD (see Figure S2b in the Supporting Information) measurements indicate different apparent pore sizes in the CNETMS films with mean values on the order of ∼10 nm, as observed by top-surface and freeze-fractured cross sectional SEM imaging, to ∼1 nm via XRD, as is typical for sol−gel films annealed at relatively low temperature (≤150 °C). High-resolution TEM images (see Figures S5 and S6 in the Supporting Information) of prepared cross sections of the CNETMS films show a dense morphology with features that are <1 nm in size, consistent with the XRD data. Although we are not certain about the origin of the larger features in the SEM images, it is possible that these features result from stresses during film processing or the fracturing process used to obtain the cross sectional SEM images.

The measured ε_r and loss tangent as a function of frequency for CNETMS films in parallel plate capacitor devices (see Figure S1b in the Supporting Information) are shown in Figure S7 in the Supporting Information. The ε_r of the CNETMS films was 20 at 1 kHz, consistent with the values for mixtures of cyanoalkyl-trialkoxysilanes reported previously.[16] The large ε_r of the CNETMS films is attributed to the orientational contribution of the dipolar cyano groups present in the sol−gel network, as will be discussed below. The pore structure of the CNETMS films may provide sufficient free volume for field induced reorientation and polarization of the cyano groups and interfacial contributions to the permittivity.[5] The measured ε_r of the CNETMS films showed only a small reduction as the frequency varied from 100 Hz to 1 MHz. However, at frequencies greater than 100 kHz, the ε_r decreases slightly while the loss tangent exhibits an increase in magnitude, indicating the onset of a dielectric resonance.[14]

The dielectric breakdown strengths of the CNETMS films were determined and analyzed using the Weibull method, as has been discussed elsewhere.[14] Briefly, the Weibull cumulative failure probability distribution (P_F) is expressed by the following equation

$$P_F(E) = 1 - \exp[-\{(E - \gamma)/\alpha\}^{\beta}] \quad (1)$$

where E is the applied electric field, α is the "scale" parameter, β is the "shape" parameter or Weibull modulus (which represents dispersion of the breakdown field) and γ is the electric field breakdown threshold parameter, which represents the field below which no observable failure occurs. Conventionally, the characteristic breakdown strength, E_{BD}, is defined as the field where P_F is 63.2%. The failure probability of the CNETMS films with different thickness as a function of the applied electric field is shown in Figure S8 in the Supporting Information. In general, the narrower the cumulative distribution function (CDF) with respect to electric field, the more reliable the material is for high dielectric strength applications.

The effect of thickness on the dielectric breakdown strength for CNETMS films is shown in Figure 1. In this graph, we plotted the average breakdown strength ($\langle E_B \rangle$) over the measured distribution of breakdown fields for a given sample. It can be seen that $\langle E_B \rangle$ increases as the thickness of the CNETMS films decreased, following an approximate inverse dependence on thickness, i.e., $\langle E_B \rangle \approx d^{-1}$, (see Figure S9 in the Supporting Information) as is typically observed for oxide and polymer thin films.[19−21] The maximum $\langle E_B \rangle$ is ∼650 V/μm for 1.3 μm thick CNETMS film. On the other hand, the Weibull modulus, β, decreases somewhat as the thickness of CNETMS is reduced, indicating a broader distribution of breakdown strength. A possible reason for this is that ionizable groups or trapped charges at the interfaces of these porous thin films may be distributed somewhat inhomogeneously.

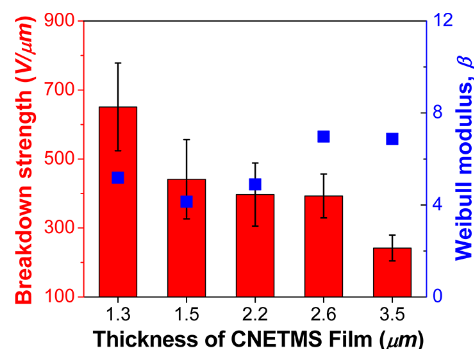

Figure 1. Thickness dependence of average breakdown strength ($\langle E_B \rangle$) and Weibull modulus for CNETMS films. The error bars represent the standard deviation (1σ) of the average breakdown strength obtained from 12 to 20 devices.

Extractable Energy Densities of CNETMS Films. To determine the maximum extractable energy density (U_{max}^{CD}) under pulsed conditions of CNETMS films, we have performed charge−discharge (C−D) measurements. As shown in Figure 2, the 3.5 μm thick CNETMS film gave a U_{max}^{CD} value of ∼4 J/cm^3, whereas the value for 1.3 μm thick CNETMS was ∼7.5 J/cm^3,

dx.doi.org/10.1021/am303162u | ACS Appl. Mater. Interfaces 2013, 5, 1544−1547

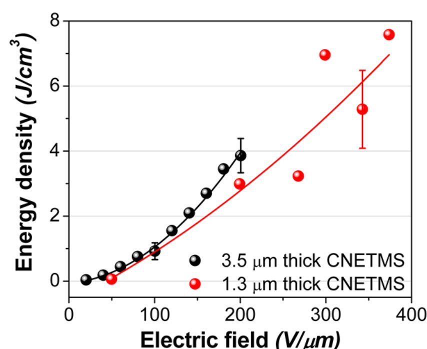

Figure 2. Extractable energy density of 3.5 and 1.3 μm thick CNETMS films from charge–discharge measurements. The error bars were obtained from measurements of 2–5 devices at the given electric field strength whereas the data points without an error bar were obtained from a single measurement at the applied electric field.

which is about twice as high as that of the thicker CNETMS film, as a result of the higher $\langle E_B \rangle$ for the thinner film. The reduction of breakdown strength in C-D measurements compared to breakdown testing (shown in Figure 1) is attributed to electrical stress during the pulsed measurement conditions and the use of a larger electrode area (0.25 mm^2 for breakdown testing and 1.0 mm^2 for C–D measurements). The solid lines in Figure 2 correspond to a quadratic fit to the measured data (average values and error bars are shown when two or three devices were measured at the same electric field). Although there are some deviations at higher fields that are likely associated with leakage currents (see Figures S10 and S11 in the Supporting Information), the increase of the extractable energy density fits reasonably well to the quadratic function, which would be expected for a linear dielectric. The lower β values of thin CNETMS films are consistent with the more scattered U_{max}^{CD} than that of thicker films, which suggests that thinner CNETMS films are more prone to catastrophic breakdown events particularly at high electric fields.

Figure 3 shows the unipolar P–E loops of 1.3 μm thick CNETMS films as a function of electric field. P-E loops

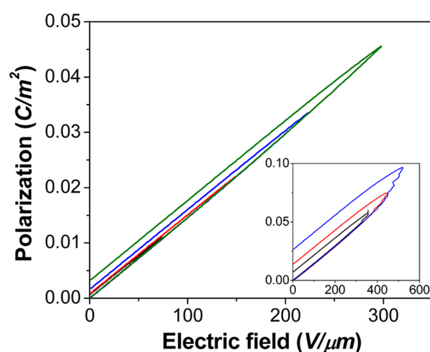

Figure 3. Polarization–electric field (P–E) loops of 1.3 μm thick CNETMS films (loops above 300 V/μm shown in the inset).

measured up to 300 V/μm display narrow loops and linear dielectric behavior, which are desirable properties in high energy storage density and low loss dielectric applications.[12] Linear dielectric polarization behavior is also observed for 3.5 μm thick CNETMS films (shown in Figure S12 in the Supporting Information) but only for fields up to ~130 V/μm. Further increases in field strength exceeding 300 V/μm (shown in the inset in Figure 3) leads to a discernible rounding of the shape of P-E loops, indicating a contribution from charge injection and conduction, which is reflected in the increased energy loss following reversal of the field.[22,23] The difference in behavior of the thin and thick films suggests that the onset of charge injection or conduction is reduced, consistent with the trend of the breakdown data, and may be associated with an increase of voids, impurities, and trapped charges in CNETMS films when the thickness is increased.

We have assessed the extractable energy density, U_{max}^{PE}, and the energy extraction efficiency from the P-E measurements on the CNETMS films by integrating the area under the charge and discharge curves[24] as shown in Figure S13 in the Supporting Information. The U_{max}^{PE} and the energy extraction efficiency of CNETMS films are shown in Figure 4. CNETMS

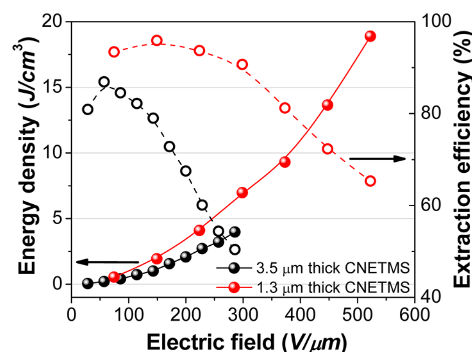

Figure 4. Extractable energy density and extraction efficiency from polarization-electric field measurements for 3.5 and 1.3 μm thick CNETMS films. Energy density and extraction efficiency are shown in solid and hollow circles, respectively.

films with a thickness of 3.5 μm exhibit a U_{max}^{PE} value of ~4 J/cm^3 at ~300 V/μm, whereas the U_{max}^{PE} of 1.3 μm thick CNETMS is determined to be ~19 J/cm^3 at ~500 V/μm, resulting from both the higher $\langle E_B \rangle$ and the energy extraction efficiency, as is indicated by narrow P-E loops, arising from the lower film thickness. It should be noted that the energy loss in dielectric capacitors will be dissipated in the form of heat, thereby limiting the efficiency and, more importantly, the lifetime of capacitors in use. Accordingly, the maximum extractable energy density of a capacitor has to be determined with due consideration of the energy extraction efficiency.

Table 1 summarizes U_{max}^{CD}, U_{max}^{PE} and the energy extraction efficiency of 1.3 and 3.5 μm thick CNETMS films. To take

Table 1. U_{max}^{CD}, U_{max}^{PE} and the Energy Extraction Efficiency of 1.3 and 3.5 μm Thick CNETMS Films

CNETMS thickness (μm)	U_{max}^{CD}(J/cm^3)	U_{max}^{PE} (J/cm^3)	energy extraction efficiency from P–E method (%)
1.3	7 ± 1 @ 300 V/μm	7.0 @ 300 V/μm	91
3.5	4 ± 1 @ 200 V/μm	2.1 @ 200 V/μm	68

extraction efficiency into account, the value of U_{max}^{PE} is chosen at a moderate electric field, 300 V/μm for 1.3 μm and 200 V/μm for 3.5 μm thick CNETMS film, respectively. U_{max}^{PE} of 3.5 μm thick CNETMS is ~2 J/cm^3 with extraction efficiency of 68%, whereas 1.3 μm CNETMS achieves 7 J/cm^3 of U_{max}^{PE} with extraction efficiency of 91%. As shown by the wide P-E loop at ~200 V/μm in Figure S12 in the Supporting Information, the

loss in 3.5 μm thick CNETMS significantly compromises the energy extraction efficiency even for moderate electric fields. On the contrary, 1.3 μm thick CNETMS maintains a high efficiency and large extractable energy at moderately high fields, as shown in both C-D and P-E measurements. Current research is aimed at the suppression of charge injection and conduction in sol−gel dielectric films to further enhance the energy storage and extraction capabilities and the device reliability.

■ CONCLUSIONS

We have shown that sol−gel dielectric films derived from a neat 2-cyanoethyltrimethoxysilane precursor and fabricated by a simple solution processing show a large relative permittivity of 20 at 1 kHz and a relatively high dielectric strength of 650 V/μm for a 1.3 μm thick film. The large relative permittivity of CNETMS films is attributed to the orientational polarization of polar cyano groups, as supported by narrow loops and linear dielectric behavior in P-E measurements up to ∼300 V/μm for CNETMS films. The combination of a dipole-reorientation polarization mechanism, sizable permittivity, and moderately high dielectric strength has led to an extractable energy density of 7 J/cm^3 and an energy extraction efficiency of ∼90% at 300 V/μm for CNETMS films. The large extractable energy density and high dielectric strength of CNETMS films suggests the potential for hybrid organic-silica sol−gel dielectric films for use in energy storage and pulsed power applications, as well as in organic electronics as a gate dielectric and a high dielectric layer for electrostatic trapping or release of charged or dielectric particles.

■ ASSOCIATED CONTENT

Supporting Information

Preparation of hybrid organic−silica sol−gel films, device fabrication, and characterization of dielectric properties, FT-IR, XRD and AFM Analysis, chemical and device structures, SEM and TEM Images of CNETMS film, dielectric spectroscopy of CNETMS films, breakdown strength distributions and thickness dependence, and current density vs field (leakage current) measurements and polarization-electric field measurements. This material is available free of charge via the Internet at http://pubs.acs.org.

■ AUTHOR INFORMATION

Corresponding Author

*E-mail: joe.perry@gatech.edu.

Notes

The authors declare no competing financial interest.

■ ACKNOWLEDGMENTS

The work of Y.K., M.K., and O.L.S. was supported by the Office of Naval Research (Grant N000141110462, Capacitor Program). The work of M.K., K.H.S., and J.W.P. was supported by the Air Force Office of Scientific Research (Grant FA9550-10-1-0555, BIO-PAINTS MURI). The work of Y.C. was supported by the Air Force Office of Scientific Research (Grant FA9550-09-1-0162, BIONIC Air Force Center of Excellence). The authors thank Prof. Kippelen for use of a profilometer and dielectric spectroscopy instruments. O.L.S. and Y.K. thank the Center for Organic Photonics and Electronics for a COPE Fellowship.

■ REFERENCES

(1) Kötz, R.; Carlen, M. *Electrochim. Acta* **2000**, *45*, 2483−2498.

(2) Goodenough, J. B.; Abruna, H. D.; Buchanan, M. V. *Basic Research Needs for Electrical Energy Storage. Report of the Basic Energy Sciences Workshop on Electrical Energy Storage, April 2−4, 2007*; DOE/SC/BES-0702; U.S. Department of Energy Office of Science: Washington, D.C., 2007.

(3) Whittingham, M. S. *MRS Bull.* **2008**, *33*, 411−419.

(4) Simon, P.; Gogotsi, Y. *Nat. Mater.* **2008**, *7*, 845−854.

(5) Wang, Q.; Zhu, L. *J. Polym. Sci., Part B: Polym. Phys.* **2011**, *49*, 1421−1429.

(6) Barber, P.; Balasubramanian, S.; Anguchamy, Y.; Gong, S.; Wibowo, A.; Gao, H.; Ploehn, H. J.; zur Loye, H.-C. *Materials* **2009**, *2*, 1697−1733.

(7) Dang, Z.-M.; Yuan, J.-K.; Zha, J.-W.; Zhou, T.; Li, S.-T.; Hu, G.-H. *Prog. Mater. Sci.* **2012**, *57*, 660−723.

(8) Sarjeant, W. J.; Zirnheld, J.; MacDougall, F. W. *IEEE Trans. Plasma Sci.* **1998**, *26*, 1368−1392.

(9) Yao, K.; Chen, S.; Rahimabady, M.; Mirshekarloo, M. S.; Yu, S.; Tay, F. E. H.; Sritharan, T.; Lu, L. *IEEE Trans. Ultrason., Ferroelectr., Freq. Control* **2011**, *58*, 1968−1974.

(10) Wang, Y.; Zhou, X.; Chen, Q.; Chu, B.; Zhang, Q. *IEEE Trans. Dielectr. Electr. Insul.* **2010**, *17*, 1036−1042.

(11) Guan, F.; Yang, L.; Wang, J.; Guan, B.; Han, K.; Wang, Q.; Zhu, L. *Adv. Funct. Mater.* **2011**, *21*, 3176−3188.

(12) Zhu, L.; Wang, Q. *Macromolecules* **2012**, *45*, 2937−2954.

(13) Kim, P.; Jones, S. C.; Hotchkiss, P. J.; Haddock, J. N.; Kippelen, B.; Marder, S. R.; Perry, J. W. *Adv. Mater.* **2007**, *19*, 1001−1005.

(14) Kim, P.; Doss, N. M.; Tillotson, J. P.; Hotchkiss, P. J.; Pan, M.-J.; Marder, S. R.; Li, J.; Calame, J. P.; Perry, J. W. *ACS Nano* **2009**, *3*, 2581−2592.

(15) Chon, J.; Ye, S.; Cha, K. J.; Lee, S. C.; Koo, Y. S.; Jung, J. H.; Kwon, Y. K. *Chem. Mater.* **2010**, *22*, 5445−5452.

(16) Maruyama, K.; Chiba, T.; Takamizawa, M. *Film capacitor.* U.S.Patent 4,843,517, June 27, 1989.

(17) Hench, L. L.; West, J. K. *Chem. Rev.* **1990**, *90*, 33−72.

(18) Novak, B. M. *Adv. Mater.* **1993**, *5*, 422−433.

(19) Lee, H.; Smith, N. J.; Pantano, C. G.; Furman, E.; Lanagan, M. T. *J. Am. Ceram. Soc.* **2010**, *93*, 2346−2351.

(20) Zhou, H.; Shi, F. G.; Zhao, B. *Microelectron. J.* **2003**, *34*, 259−264.

(21) Kim, H. K.; Shi, F. G. *IEEE Trans. Dielectr. Electr. Insul.* **2001**, *8*, 248−252.

(22) Chen, Q.; Wang, Y.; Zhou, X.; Zhang, Q. M.; Zhang, S. *Appl. Phys. Lett.* **2008**, *92*, 142909.

(23) *IEEE Standard Definitions of Primary Ferroelectric Terms 180−1986*; IEEE: New York, 1986.

(24) Chu, B.; Zhou, X.; Ren, K.; Neese, B.; Lin, M.; Wang, Q.; Bauer, F.; Zhang, Q. M. *Science* **2006**, *313*, 334−336.